CMS Physics Analysis Summary

Contact: cms-pog-conveners-tau@cern.ch 2011/03/18

Performance of tau reconstruction algorithms in 2010 data collected with CMS

The CMS Collaboration

Abstract

Proton–proton collision events collected with the CMS experiment at LHC at a center–of–mass energy of 7 TeV in 2010 and corresponding to an integrated luminosity of 36 pb^{-1} are used to measure the performance of reconstruction and identification of tau lepton hadronic decays.

1 Introduction

Tau leptons play a significant role in physics analyses performed by the CMS experiment. Studies covering diverse topics ranging from electroweak measurements to searches for Higgs bosons, supersymmetric particles and other new physics phenomena benefit from efficient tau reconstruction and powerful background rejection.

In about two thirds of cases taus decay hadronically, typically into either one or three charged mesons (predominantly π^+, π^-) in the presence of up to two neutral pions, decaying via $\pi^0 \rightarrow \gamma\gamma$, and a tau neutrino. This leads to an experimental signature that is similar to that expected for quark and gluon jet production. Due to the large jet–production cross section, the experimental challenge in reconstructing and identifying hadronic tau decays is to discriminate efficiently between them and jets misreconstructed as tau candidates.

This paper extends the previous study [1] and provides a reference for CMS 2010 tau–based analyses which require an estimate of the tau efficiency and fake–rate, a probability for quark and gluon jets to be misidentified as hadronic taus. This paper uses cuts which are most commonly used in the Standard Model (SM) and Higgs analyses and compares the data to predictions of the Pythia and POWHEG Monte Carlo (MC) simulation. The results are presented in terms of MC expected values and DATA to MC ratios which makes them more generally applicable, also in analyses with different event selection requirements. Since no significant differences between Pythia and POWHEG predictions were observed the MC in the paper refers to predictions of the Pythia simulation.

2 CMS detector

A detailed description of CMS can be found elsewhere [2]. The central feature of the CMS apparatus is a superconducting solenoid, of 6 m internal diameter, 13 m in length, providing a field of 3.8 T. Within the field volume are the silicon pixel and strip tracker, the crystal electromagnetic calorimeter (ECAL) and the brass/scintillator hadron calorimeter (HCAL). Muons are measured in gas-ionization detectors embedded in the steel return yoke of the solenoid. The most relevant sub-detectors for this measurement are the ECAL and the tracking system. The electromagnetic calorimeter consists of nearly 76 000 lead tungstate crystals which provide coverage in pseudorapidity $|\eta| < 1.479$ in the barrel region and $1.479 < |\eta| < 3.0$ in two endcap regions. The ECAL has an energy resolution of better than 0.5% for unconverted photons with transverse energies above 100 GeV. The inner tracker measures charged particles within the $|\eta| < 2.5$ pseudorapidity range. It consists of 1440 silicon pixel and 15148 silicon strip detector modules and is located in the 3.8 T field of the superconducting solenoid. It provides an impact parameter resolution of $\approx 15\mu m$ and a transverse momentum, p_{T}, resolution of about 1.5% for 100 GeV/c particles. The origin of the CMS coordinate system is at the nominal interaction point with the Z axis along the beams direction pointing west, X axis pointing towards the center of LHC and Y axis pointing upwards.

3 CMS tau reconstruction algorithms

The optimization of the tau identification performance in terms of efficiency and the fake–rate is achieved by analyzing the constituents of jets in order to identify specific individual tau hadronic decay modes. The majority of tau decays proceeds through intermediate resonances, therefore the hadronic tau identification can be reframed from a search for collimated hadron jets satisfying the tau mass constraint into an ensemble of searches for production of the differ-

ent hadronic tau decay resonances.

CMS developed two main tau reconstruction algorithms : Tau Neural Classifier (TaNC) and Hadron plus Strips (HPS). Both algorithms use Particle Flow (PF) [3] objects. In the PF approach the information from all sub-detectors is combined to identify and reconstruct all particles produced in the collision, namely charged hadrons, photons, neutral hadrons, muons, and electrons. The resulting list of particles is used to construct taus. The hadronic taus in this analysis use only visible products of tau decays, neutrinos are not considered. One of the major tasks in reconstructing the decay mode of the tau is determining the number of π^0 mesons produced in the decay. The TaNC attempts to reconstruct the best π^0 candidate based on the existing PF photon candidates, whereas the HPS combines PF electromagnetic particles in "strips", to take into account possible broadening of calorimeter depositions from photon conversions. The neutral objects are then combined with existing charged hadrons to reconstruct the hadronic tau decay products.

After the decay mode of the tau candidate has been reconstructed, the TaNC algorithm feeds the tau candidate to an ensemble of neural networks, each corresponding to one of the five dominant hadronic decay modes. By adjusting the thresholds of cuts on the neural network output three "working points": "loose","medium" and "tight" were defined.

In the case of HPS if more than one hypothesis for possible tau decay signatures exists the hypothesis leading to the lowest E_T sum of jet constituents not associated to tau decay products is given preference. Finally, reconstructed candidates are required to satisfy isolation criteria which are based on counting the number of charged hadrons and photons above a certain E_{T} threshold, not associated to the tau decay signature within an isolation cone of size $\Delta R = 0.5$. Three sets of E_{T} thresholds define "loose", "medium" and "tight" "working points". A detailed description of the algorithms can be found elsewhere [1].

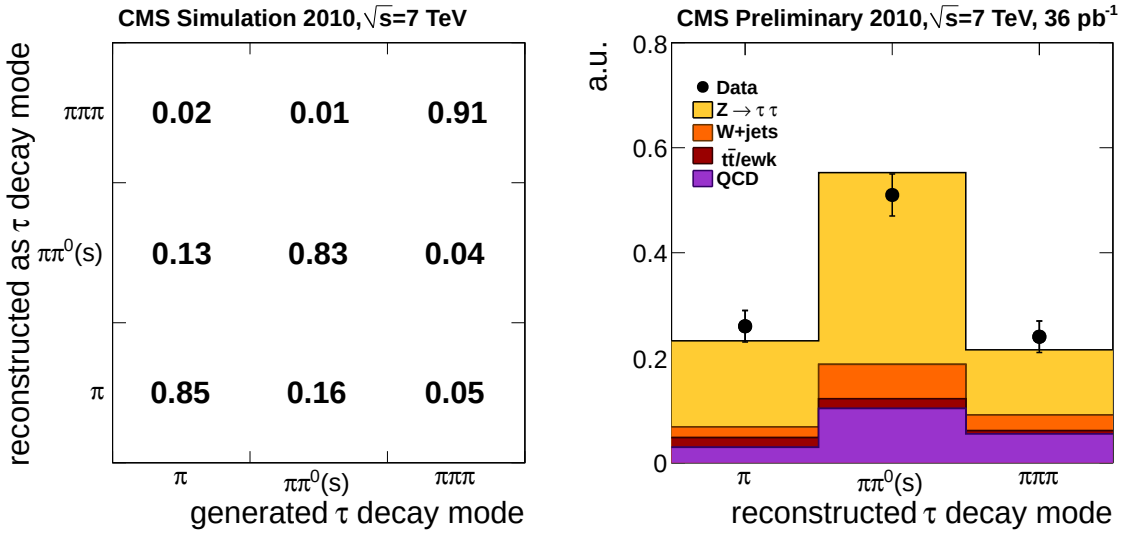

Figure 1: (left) The plot shows a fraction of generated taus of a given type reconstructed in a certain decay mode for the HPS "loose" working point and a sample of $Z \to \tau^+\tau^-$ simulated MC events. (right) The plot represents data to MC comparison for number of taus reconstructed in different tau decay modes using a data sample of $Z \to \tau^+\tau^- \to \mu\tau_{had}$ events. The MC is a mixture of the signal and background MC samples based on the corresponding cross sections.

A correlation between generated and reconstructed tau decay modes was studied using a sam-

ple of simulated $Z \to \tau_{had}\tau_{had}$ MC events, where τ_{had} denotes the taus decaying hadronically. The results are presented in Fig. 1 left. Each column reproduces one generated decay mode normalized to unity. The y-axis represents the fraction of generated taus of a given type reconstructed in a certain decay mode. Both generated and reconstructed taus were required to have a visible transverse momentum, $p_{\mathrm{T}}^{\tau_{had}} > 15$ GeV, and to match within a cone of $\Delta R < 0.15$, where $\Delta R = \sqrt{(\eta^{gen}_{\tau_{had}} - \eta^{rec}_{\tau_{had}})^2 + (\phi^{gen}_{\tau_{had}} - \phi^{rec}_{\tau_{had}})^2}$, where η and ϕ are pseudorapidity and azimuthal angles of reconstructed and generated taus. The correlation between generated and reconstructed decay modes exceeds 80% even for decays including neutral pions and reaches 90% for three charged pion decay mode.

A data to MC comparison of the number of events reconstructed in different tau–decay modes was performed using a sample of $Z \to \tau\tau \to \mu\tau_{had}$ events selected using cuts described elsewhere [4], and is shown in Fig. 1 right. The taus were required to have visible transverse momenta $p_{\mathrm{T}}^{\tau_{had}} > 20$ GeV within the geometric acceptance $|\eta_{\tau_{had}}| < 2.3$. The MC sample represents a mixture of the signal and background MC samples based on the corresponding cross sections. The performance of the tau algorithm in data is well reproduced by predictions of the MC simulation.

4 Efficiency of tau reconstruction and identification.

To measure the efficiency of tau reconstruction and identification in data, a sample of $Z \to \tau\tau \to \mu\tau_{had}$ events enriched in real taus was used with relatively small contribution from other processes. The events were preselected using kinematic cuts and a set of requirements to suppress the background from $Z \to \mu\mu$, W and QCD events, but without applying the tau identification algorithms. The preselection requires the event to be triggered by a single muon trigger, to contain only one isolated muon with $p_{\mathrm{T}}^{\mu} > 15$ GeV within the geometric acceptance $|\eta_{\mu}| < 2.1$, an isolated tau–jet candidate of $p_{\mathrm{T}}^{\tau_{had}} > 20$ GeV within the geometric acceptance $|\eta_{\tau_{had}}| < 2.3$, and a "leading" (highest p_{T}) track within the jet with $p_{\mathrm{T}} > 5$ GeV. The tau–jet (τ_{jet}) four-momentum is reconstructed using the anti–k_T algorithm in a cone of size 0.5 [5] and is required to fail an electron discriminator. The muon and the "leading" track are required to be of opposite charge. To suppress the background contribution an additional requirement on transverse mass, $M_T < 40$ GeV, was applied. The transverse mass is defined as $M_T = \sqrt{2p_{\mathrm{T}}^{\mu}E_{\mathrm{T}}^{miss} \cdot (1 - \cos\Delta\phi)}$, where p_{T}^{μ} is the muon transverse momentum, E_{T}^{miss} is the PF missing transverse energy and $\Delta\phi$ is the azimuthal angle between the missing transverse energy vector and the muon transverse momentum vector.

Both TaNC and HPS were run on the preselected events. The resulting visible invariant mass distributions of the $\mu\tau_{jet}$ system for those events which pass or fail the tau identification were fitted using signal and background templates provided by Monte Carlo simulation. The efficiency was then calculated as: $\varepsilon = N^{Z\to\tau\tau}_{pass}/(N^{Z\to\tau\tau}_{pass} + N^{Z\to\tau\tau}_{fail})$, where $N^{Z\to\tau\tau}_{pass,fail}$ is the number of tau events after background contributions were subtracted. Figure 2 shows visible invariant mass of the $\mu\tau_{jet}$ system for preselected events which passed (left) and failed (right) the "loose" tau identification requirements. Since in the "failed" sample there is no tau reconstructed, to make the plots consistent the visible mass is always computed using the jet four–vector for taus and not the tau four–vector as reconstructed by identification algorithms. The MC predictions for signal and background events are also shown. The MC describes data well in the "pass" region which has a well defined shape dominated by Z events and a small background contribution. The sample of "failed" events is dominated by background contributions. The MC predictions describe data reasonably well. The stability of the fit results were tested by using

data driven background estimates instead of the MC templates and by varying invariant mass ranges for the fit. All checks demonstrated consistent results within the uncertainties of the method.

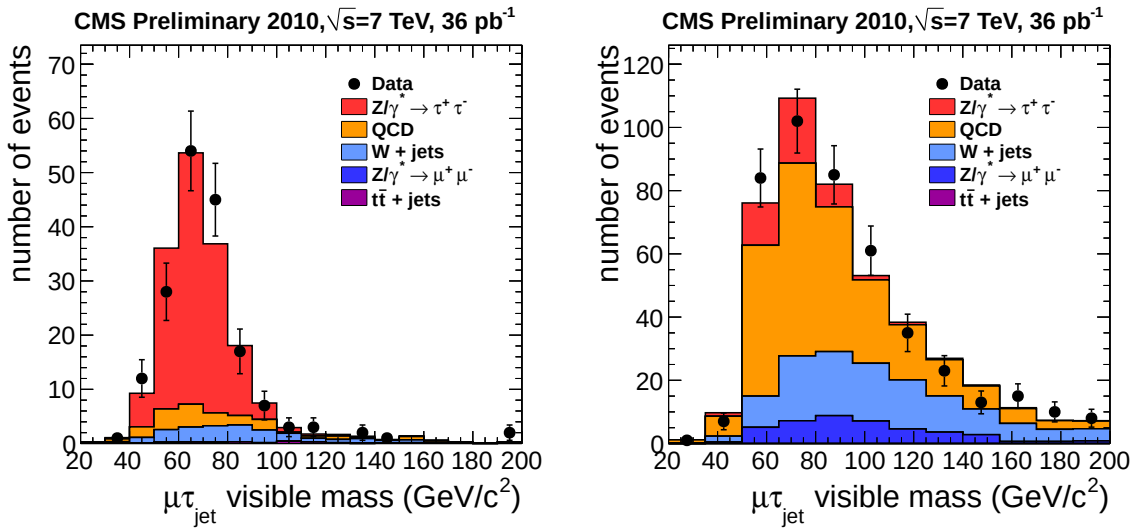

Figure 2: The visible invariant mass of the $\mu\tau_{jet}$ system for preselected events which passed (left) and failed (right) the HPS "loose" tau identification requirements compared to predictions of the MC simulation.

Algorithm	Fit data	Expected MC	DATA/MC
TaNC "loose"	0.76 ± 0.20	0.72	1.06 ± 0.30
TaNC "medium"	0.63 ± 0.17	0.66	0.96 ± 0.27
TaNC "tight"	0.55 ± 0.15	0.55	1.00 ± 0.28
HPS "loose"	0.70 ± 0.15	0.70	1.00 ± 0.24
HPS "medium"	0.53 ± 0.13	0.53	1.01 ± 0.26
HPS "tight"	0.33 ± 0.08	0.36	0.93 ± 0.25
HPS "loose"	combined fit [4]		0.94 ± 0.09
HPS "loose"	$\tau\tau$ to $\mu\mu, ee$ fit [4]		0.96 ± 0.07

Table 1: Efficiency for hadronic tau decays to pass TaNC and HPS tau identification criteria measured by fitting the $Z \to \tau^+\tau^-$ signal contribution in the samples of the "passed" and "failed" preselected events. The errors of the fit represent statistical uncertainties. The last column represents the data to MC correction factors and their full uncertainties including statistical and systematic components. Data to MC ratios for the tau reconstruction efficiency measured using fits to the measured Z production cross sections as described in [4] are also shown.

Results of the fits are summarized in Table 1. The values measured in data, "Fit data" are compared with the expected values, "Expected MC", obtained by repeating the fitting procedure on simulated events. The performance of the tau algorithms on preselected events is expected to be approximately 30% higher than for an inclusive sample of taus, without pre-selection. In general the absolute value of the efficiency depends on p_{T} and η requirements, which are applied in each individual physics analysis, therefore the main goal of this measurement is to perform the data to MC comparison and to determine data to MC correction factors and their uncertainties. With the current data sample the statistical uncertainties of the fits are in the

range of 20%-30% whereas the agreement in the mean values of the fits between data and MC was observed to be better than few percent.

Systematic uncertainties on the measured tau identification efficiencies arise from uncertainties on track reconstruction, 4%, and from uncertainties on the probabilities for tau–jets to pass the "leading" track p_{T} and loose isolation requirements applied in the preselection, up to 12%. Uncertainties on track momentum and tau–jet energy scales have an effect on the measured tau identification efficiencies below 1%. All numbers represent relative uncertainties.

The resulting ratio of the measured efficiencies to those predicted by MC for hadronic tau decays to pass the "loose", "medium" and "tight" TaNC and HPS working points are presented in the last column of Table 1. The uncertainties of the ratios represent the full uncertainties of the method which are calculated by adding statistical and systematic uncertainties in quadrature. The total uncertainty of the measured efficiency of the tau algorithms is dominated by the statistical uncertainty of the fit. The simulation describes the data well, the differences between measured efficiencies in data and those estimated using MC samples are much smaller than the measured experimental uncertainties. Since the same event sample was used to evaluate efficiencies for different working points the results are correlated.

A complementary method to estimate the uncertainty of the tau reconstruction and identification efficiency with higher precision uses a comparison between the observed number of $Z \to \tau\tau$ events in different decay modes and $Z \to \mu\mu$ events as described elsewhere [4]. The first approach is using a simultaneous fit of all four $Z \to \tau\tau$ decay channels with final states $\mu\mu, e\mu, \mu\tau_{had}$ and $e\tau_{had}$. As a result of the fit a combined cross section and a tau efficiency are measured. The data to MC correction factor for the HPS "loose" working point was measured to be 0.94 ± 0.09. The second approach is based on comparison of only hadronic tau channels, $Z \to \mu\tau_{had}$ and $e\tau_{had}$, to combined $Z \to \mu\mu, ee$ cross section as measured by CMS. The data to MC correction factor for the HPS "loose" working point in this case was measured to be 0.96 ± 0.07. A slightly better uncertainty of the latter method is explained by a high precision of the combined $Z \to \mu\mu, ee$ cross section measurement. These values are also presented in Table 1 for comparison.

The expected efficiency values for hadronic taus from $Z \to \tau\tau$ process to be reconstructed with $p_{\mathrm{T}}^{\tau_{had}} > 15$ GeV and $p_{\mathrm{T}}^{\tau_{had}} > 20$ GeV and $|\eta_{\tau_{had}}| < 2.3$ were estimated using simulated events and are presented in Table 2. The cuts were applied both at the generated and reconstructed level. A matching, $\Delta R < 0.15$, between generated and reconstructed taus was required. Figure 3 represents the expected efficiencies as a function of the generated visible tau p_{T} for all working points of each algorithm.

Algorithm	TaNC			HPS		
	"loose"	"medium"	"tight"	"loose"	"medium"	"tight"
Efficiency ($p_{\mathrm{T}}^{\tau_{had}} > 15$ GeV)	53.6%	43.1%	30.4%	45.9%	33.8%	22.9%
Efficiency ($p_{\mathrm{T}}^{\tau_{had}} > 20$ GeV)	57.8%	47.9%	35.6%	49.9%	36.5%	24.6%

Table 2: The expected efficiency for hadronic tau decays to pass TaNC and HPS tau identification criteria estimated using $Z \to \tau\tau$ events simulated using MC for two different cuts on the visible p_{T} of the taus.

5 Tau energy scale

Since hadronic taus consist of charged hadrons and photons reconstructed with a high precision using the PF techniques the reconstructed tau energy is expected to be close to the true

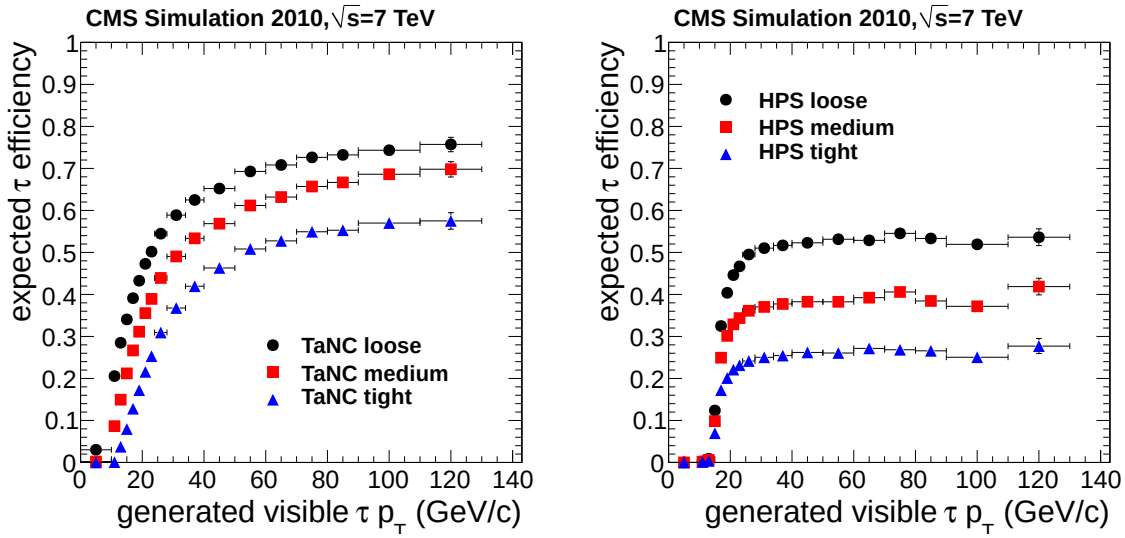

Figure 3: The expected efficiency of the tau algorithms as a function of generated visible tau p_{T} estimated using a sample of simulated $Z \to \tau\tau$ events for the TaNC (left) and HPS (right) algorithms.

energy of the visible tau decay products. According to simulation, the ratio of the reconstructed to the true visible tau energy for the HPS algorithm is constant and within 2% from unity, while for TaNC it decreases by about 2% towards $p_{\mathrm{T}}^{\tau} = 60$ GeV/c. The η dependence is more pronounced. For both algorithms the reconstructed tau energy degrades with respect to the true one by moving from the central, barrel, to endcap region by about 5%.

It is expected that the p_{T} and η-dependent behavior of the tau response is well reproduced by the MC simulation, and that the ratio of the tau response in data to the response in MC is very close to unity. The quality of the tau energy scale simulation can be examined by analyzing the $Z \to \tau^{+}\tau^{-} \to \mu\tau_{had}$ data sample, assuming that the tautau mass spectrum is not altered significantly by non-SM sources of $\tau\tau$ events. The visible invariant mass of the $\mu\tau_{had}$ system is very sensitive to the energy scale of the τ, since the muon four–momenta are measured with a high precision. By varying the tau energy scale simultaneously in the signal and background MC samples a set of templates was produced. The resulting templates were fit to the data and the best agreement was achieved by scaling the tau energy in simulation by a factor 0.97 ± 0.03, where the uncertainty of the tau energy scale is averaged over the pseudorapidity range of the data sample.

A complementary procedure, which does not assume knowledge of the $\tau\tau$ invariant mass spectrum, was based on the invariant mass of reconstructed tau decays and is shown in Fig. 4. The method uses taus as standalone objects but still relies on good understanding of underlying background events which contribute to the signal sample. The fit was performed separately for $\pi\pi^0$ and $\pi\pi\pi$ decay channels, since the major source of the uncertainty is expected to come from reconstruction of the electromagnetic energy. The simulation describes both decay channels well. The data to MC ratio was measured to be 0.97 ± 0.03 for the $\pi\pi^0$ decay mode and 1.01 ± 0.02 for the $\pi\pi\pi$ decay mode. The effect of the energy scale uncertainty on the shape of the tau invariant mass is also illustrated in Fig. 4. Varying the energy scale in simulation by the uncertainty delivered from the $\mu\tau_{had}$ invariant mass fit, 3%, leads to a significant deviation in the predicted mass shapes of taus.

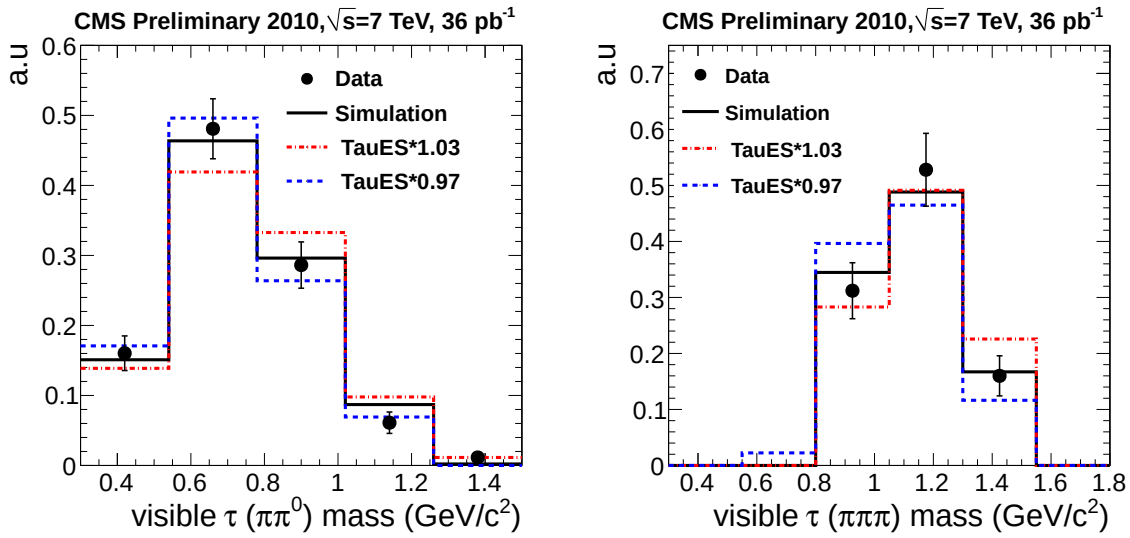

Figure 4: The reconstructed invariant mass of taus decaying into one charged and one neutral pion (left) and into three charged pions (right) compared to predictions of the simulation. The black lines represent results of the fit and the dashed lines represent the predictions with tau energy scale, TauES, varied up and down by 3%.

6 Fake–rate measurement

The major sources of jets which can fake hadronic taus are jets produced in QCD processes and jets produced in association with Z and W bosons. The QCD–type jets were selected using events with at least one jet of transverse momentum $p_{\mathrm{T}}^{jet} > 15$ GeV and a jet of $p_{\mathrm{T}}^{jet} > 10$ GeV within $|\eta| < 2.5$. For Z and W type jet events were selected with at least one isolated muon with transverse momentum $p_{\mathrm{T}}^{jet} > 15$ GeV and $|\eta| < 2.1$ and a jet of transverse momentum $p_{\mathrm{T}}^{jet} > 10$ GeV within $|\eta| < 2.5$. In addition, a muon–enriched QCD sample was selected requiring a muon and a jet but suppressing the W contribution by selecting events with $M_T < 40$ GeV. For each of these samples additional cuts were also applied to suppress the background contribution from events with jets of other types.

Figure 5 shows the fake–rate as a function of the jet p_{T} for the "loose" working points of the TaNC and HPS algorithms, where the the measured values are compared with the MC predictions for the different type of jets. The values of the fake–rates expected from simulation and the measured data to MC ratios integrated over the p_{T} and η phase space used in the $Z \to \tau\tau$ analysis, $p_{\mathrm{T}}^{jet} > 20$ GeV and $|\eta| < 2.3$, are summarized in Table 3 for the three working points of both reconstruction algorithms. The fake–rate as a function of efficiency for all working points for both algorithms is shown in Fig. 6, which summarizes the MC estimated efficiency and the measured fake–rate values presented in Tables 5 and 2. Since the QCD and QCD μ-enriched fake–rates values were observed to be similar only one set of QCD points is shown. Open symbols represent results obtained by running a fixed cone algorithm based on the PF taus on simulated events only. The algorithm is effectively the same which was used in the CMS physics technical design report (PTDR) and is shown for comparison.

Isolated electrons passing the identification and isolation criteria of the tau algorithms are also an important source of background to many analyses with taus in the final state. In this case the electron is misidentified as a pion originating from the hadronic decay of the tau. A multivariate discriminator is used to reduce this background improving the pion/electron separation.

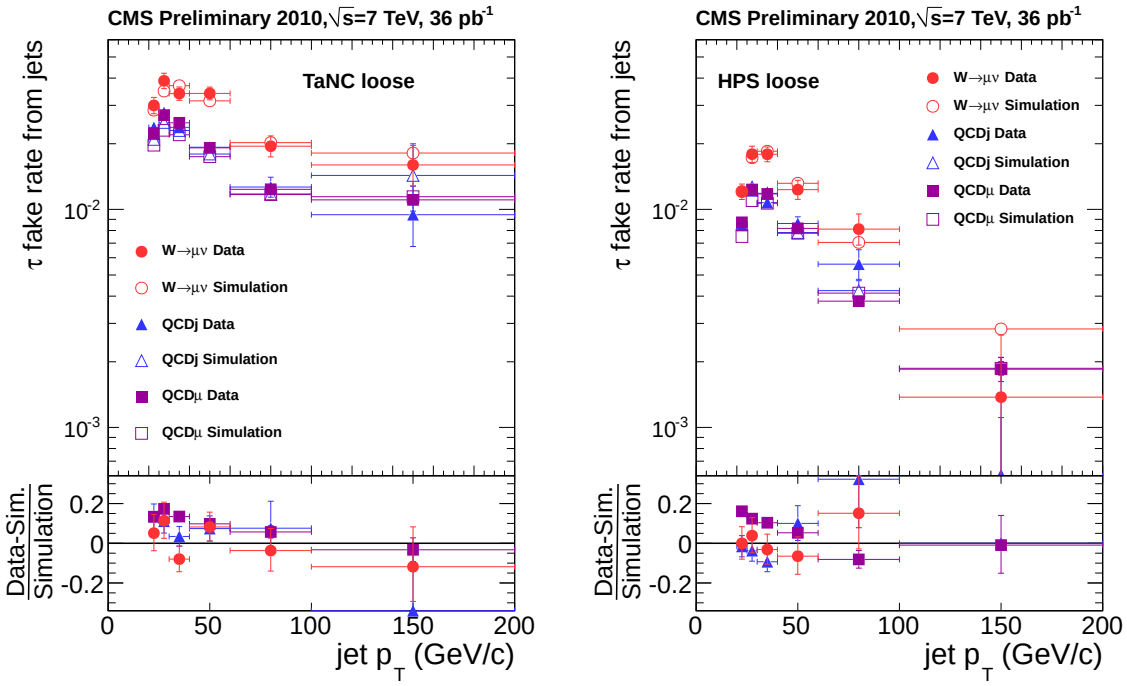

Figure 5: Probabilities of quark and gluon jets to pass "loose" working points of the TaNC (left) and HPS (right) algorithms as a function of jet p_T for QCD, QCD μ-enriched and W type events. Fake-rate measured in data are represented by solid symbols and compared to MC prediction represented by open symbols.

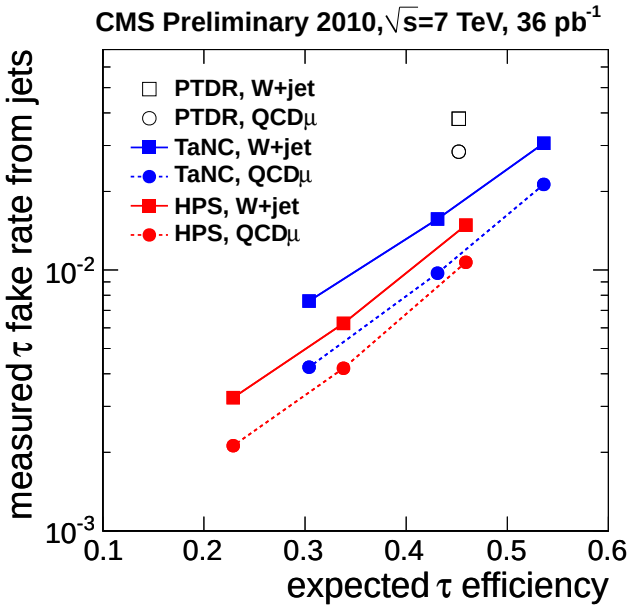

Figure 6: The measured fake–rate as a function of MC estimated efficiency for all working points for QCD μ-enriched and W data samples. The PTDR points represent results of the fixed cone algorithm based on the PF taus.

Algorithm	QCDj		QCDμ		W + jets	
	MC	DATA/MC	MC	DATA/MC	MC	DATA/MC
TaNC "loose"	2.1%	1.05 ± 0.04	1.9%	1.12 ± 0.01	3.0%	1.02 ± 0.05
TaNC "medium"	1.3%	1.05 ± 0.05	0.9%	1.08 ± 0.02	1.6%	0.98 ± 0.07
TaNC "tight"	0.5%	0.98 ± 0.07	0.4%	1.06 ± 0.02	0.8%	0.95 ± 0.09
HPS "loose"	1.0%	1.00 ± 0.04	1.0%	1.07 ± 0.01	1.5%	0.99 ± 0.04
HPS "medium"	0.4%	1.02 ± 0.06	0.4%	1.05 ± 0.02	0.6%	1.04 ± 0.06
HPS "tight"	0.2%	0.94 ± 0.09	0.2%	1.06 ± 0.02	0.3%	1.08 ± 0.09

Table 3: The MC expected fake–rate values and the measured data to MC ratios integrated over the p_{T} and η phase space typical for the $Z \to \tau\tau$ analysis.

The same discriminator, implemented as a Boosted Decision Tree is used in the PF algorithm and its output is denoted by ξ following the notation in [6].

Two selected working points, corresponding to $\xi < -0.1$ and $\xi < 0.6$ are considered in this analysis. The first working point is optimized for a low fake–rate, $O(2\%)$, at the price of about 4% losses of real hadronic taus. The second working point suffers from larger fake-rates ($O(20\%)$) since it was optimized for efficiencies on hadronic taus exceeding 99.5%.

To estimate the $e \to \tau_{had}$ fake-rate a sample of isolated electrons coming from the decay of the $Z \to ee$ resonance was selected. The electron which is used as a tag, is required to be isolated and to have a p_{T} in excess of 25 GeV. The second electron, a probe, is required to pass all tau-identification and isolation discriminators, without requiring any specific veto against electrons. The ratio between the number of probes passing the anti-electron discriminator to the overall number of selected probes is an estimator of the $e \to \tau_{had}$ fake–rate. To remove a contamination from the fake electrons a background-subtraction procedure is performed by fitting the passing and failing mass distributions to the superimposition of a signal and background components.

Table 4 shows the ratio between fake-rates as measured in the data and those obtained using MC for two $|\eta|$ bins. In the central η region the simulation underestimates the measured fake–rate values. Within the uncertainties of the measurement values for both discriminators agree in the same η intervals. The results of tag and probe method applied to the MC are also shown.

bin	discriminator by $\xi < -0.1$			discriminator by $\xi < 0.6$		
$\lvert\eta\rvert$	MC(exp),%	MC(t&p),%	DATA/MC	MC(exp),%	MC(t&p),%	DATA/MC
< 1.5	2.22 ± 0.03	2.21 ± 0.05	1.13 ± 0.17	13.19 ± 0.06	13.10 ± 0.08	1.14 ± 0.04
> 1.5	3.90 ± 0.06	3.96 ± 0.09	0.82 ± 0.18	26.90 ± 0.13	26.80 ± 0.16	0.90 ± 0.04

Table 4: The expected MC values of the fake–rates and measured ratio of the data to MC response.

7 Conclusions

The performance of two tau reconstruction algorithms developed by CMS, TaNC and HPS, has been studied using the data sample collected with the CMS detector at a center-of-mass energy of 7 TeV in 2010 and corresponding to an integrated luminosity of 36 pb^{-1}. Both algorithms demonstrated an excellent performance in terms of identification efficiency for the hadronic decays of taus, approximately 50%, while keeping the tau fake–rate from jets at a level of ~ 1 %. The MC simulation was found to describe the data well. The tau identification efficiency uncertainty was measured to be 24 % using a tag-and-probe method in $Z \to \tau\tau \to \mu\tau_{had}$ data

sample and could be further reduced to a precision of ~ 7 % by using a global fit to all $Z \to \tau\tau$ decay channels and constraining it to the measured combined $Z \to \mu\mu, ee$ cross section. The tau energy scale was found to be close to unity with the measured energy scale uncertainty better than 3 %.

References

[1] CMS Collaboration, "Study of tau reconstruction algorithms using pp collision data collected at $\sqrt{(s)} = 7$ TeV", *CMS PAS* **PFT-10-004** (2010).

[2] CMS Collaboration, "The CMS experiment at the CERN LHC", *JINST* **0803** (2008). doi:10.1088/1748-0221/3/08/S08004.

[3] CMS Collaboration, "Commissioning of the particle flow reconstruction in minimum-bias and jet events from pp collision collected at $\sqrt{(s)} = 7$ TeV", *CMS PAS* **PFT-10-002** (2010).

[4] CMS Collaboration, "Measurement of the Inclusive $Z \to \tau\tau$ Cross Section in pp collision at $\sqrt{(s)} = 7$ TeV", *to be published*.

[5] G. P. S. M. Cacciari and G. Soyez, "The anti-kt jet clustering algorithm", *JHEP* **04** (2008) 063, arXiv:0802.1189.

[6] CMS Collaboration, "Particle-flow commissioning with muons and electrons from J/Psi and W events at 7 TeV", *CMS PAS* **PFT-10-003** (2010).